

# Characterization of the continuum and kinematical properties of nearby NLS1

Gabriel A. Oio<sup>1</sup>, Luis R. Vega<sup>1,2</sup>, Eduardo O. Schmidt<sup>1,2</sup>, and Diego Ferreira<sup>1,2</sup>

<sup>1</sup> Instituto de Astronomía Teórica y Experimental (IATE), CONICET - UNC, Laprida 854, X5000BGR, Córdoba, Argentina

<sup>2</sup> Observatorio Astronómico, Universidad Nacional de Córdoba, Laprida 854, X5000BGR, Córdoba, Argentina.

April 24, 2022

## ABSTRACT

**Aims.** In order to study the slope and strength of the non-stellar continuum, we analyzed a sample of nearby Narrow Line Seyfert 1 (NLS1). Also, we re-examined the location of NLS1 galaxies on the  $M - \sigma$  relation using the stellar velocity dispersion and the [OIII] $\lambda$ 5007 emission line as surrogate of the former.

**Methods.** We studied spectra of a sample of 131 NLS1 galaxies taken from the Sloan Digital Sky Survey (SDSS) DR7. We approached the determination of the non-stellar continuum using the spectral synthesis technique using the code STARLIGHT, adopting a power-law base to model the non-stellar continuum. A composite spectra of NLS1 galaxies was also obtained based on the sample. In addition, we obtained the stellar velocity dispersion from the code and by measuring Calcium II Triplet absorption lines and [OIII] emission lines. From Gaussian decomposition of the  $H\beta$  profile we calculated the black hole mass.

**Results.** We obtained a median slope of  $\beta = -1.6$  with a median fraction of contribution of the non-stellar continuum to the total flux of 0.64. We determined black hole masses in the range of  $\log(M_{BH}/M_{\odot}) = 5.6 - 7.5$  in agreement with previous works. We found a correlation between the luminosity of the broad component of  $H\beta$  and black hole mass with the fraction of power law component. Finally, according to our results, NLS1 galaxies in our sample follow the relation  $M - \sigma$ , both considering the stellar velocity dispersion ( $\sigma_{*}$ ), and the core component of [OIII] $\lambda$ 5007.

**Key words.** galaxies: active – galaxies: Seyfert – galaxies: nuclei – galaxies: kinematics and dynamics

## 1. Introduction

A characteristic feature of active galactic nuclei (AGN) is the presence of energy outputs which are not related to ordinary stellar processes (Lynden-Bell 1969). The presence of a non-stellar component is evident in AGN spectra, and it is frequently expressed in the form of a power-law  $f_{\lambda} \propto \lambda^{\beta}$ . Though a raw approximation, this expression resulted very useful to describe the continua of AGN. For low redshift AGN, a value of  $\beta = -1.3$  was adopted in the '80s (e.g., Richstone & Schmidt 1980; O'Brien et al. 1988; Sargent et al. 1989), and later a harder slope with  $\beta = -1.7$  was claimed (Neugebauer et al. 1987; Francis et al. 1991). Through accurate NIR-optical photometry for a sample of bright QSOs at  $z \sim 2$ , Francis (1996) determined a median slope of  $\beta = -1.65$ , which is consistent with the free-free emission models of Barvainis (1993). For high-redshift quasars the disparity in the determination of  $\beta$  is critical, as it introduces uncertainties in their measured evolution, as was pointed out by Francis (1996). For instance, an adopted value of  $\beta = -1.7$  instead of  $-1.5$  implies that, due to difference in  $k$ -corrections, the luminosity function should be incremented by a factor of 2 at  $z \sim 2$ , thus altering the inferred evolution of QSO number densities (Giallongo & Vagnetti 1992; Wisotzki 2000).

Most of the aforementioned determinations of the non-stellar continuum was made through photometry for quasars and in the UV range. Besides that, spectral measurements were done in order to characterize the continua of AGNs. By creating composite quasar spectra, Vanden Berk et al. (2001), obtain slopes of

$\beta = -1.54$  and  $-0.42$  for UV and optical ranges, respectively. Davis et al. (2007) obtained mostly in the range  $\sim -1.5$  to  $-2$ , but restricted to the UV range. Despite these important efforts, there were few works lately focused on the determination of the spectral index in the optical for low-redshift AGNs, and generally the classical value of  $\beta = -1.5$  is still widely adopted (An et al. 2013; Wang et al. 2009; Yuan et al. 2008). An exception constitutes the recent spectral analysis of Calderone et al. (2017), who obtained spectral slopes for SDSS spectra; however, they assume a fixed value of  $\beta = -1.7$  for low-redshift ( $z \leq 0.6$ ) AGNs due to the difficulty of separating stellar and non-stellar components in AGNs closer than  $z \sim 0.7$ . The presence of the stellar contribution in the measured flux of nearby AGNs is an important caveat in the determination of the spectral index indeed. When performing spectroscopy, this contribution will strongly depend on which fraction of the galaxy is observed, which in turns depends on the width of the fiber used (or slit and corresponding spectral extraction), and so on the distance of the observed galaxy. As an example, an extraction of 1 arcsec wide in a galaxy at 100 Mpc corresponds to a projected distance of about 500 pc, whilst for further galaxies we would be mapping a region of several kpc. Thus, in order to determine the non-stellar continuum it is necessary to properly discount the stellar contribution corresponding to those regions. This effect may only be minimum for luminous bright QSOs, for which the brightness is so high that the emission from their host galaxy could be neglected (Francis 1996; Davis et al. 2007; Donley et al. 2010; Donoso et al. 2018), but

for lower luminosity AGNs care must be taken when assuming this.

Narrow Line Seyfert 1 galaxies (NLS1; Osterbrock & Pogge 1985; Goodrich 1989) are an interesting subclass of AGN with relatively narrow widths of permitted optical emission lines. These galaxies are defined from their optical spectral characteristics: full width at half maximum (FWHM) of  $H\beta \leq 2000 \text{ km s}^{-1}$ , ratio  $[OIII]\lambda 5007/H\beta \leq 3$  and strong FeII multiplets (see Komossa 2008 for a review). In this paper we focus on the determination of the spectral index of the non-stellar continuum in NLS1, as well as the stellar and non stellar contributions to the total emission observed in the optical range.

For NLS1s the less massive black holes (BH) were obtained associated to the highest accretion rates, suggesting that they might be in the early stage of AGN evolution (Grupe et al. 1999; Mathur 2000a,b; Wang & Zhang 2007). The well-known scaling relation between black hole mass and host galaxy stellar velocity dispersion ( $M_{BH} - \sigma_*$ ) may indicate a co-evolution of black hole and galaxy (Ferrarese & Merritt 2000; Kormendy & Ho 2013). For NLS1s this behaviour has been explored with diverse results by many authors. While normal galaxies and AGN have similar slopes in this relation, NLS1s seem to deviate from it in the sense that they should have smaller black hole masses for a given stellar velocity dispersion (Mathur et al. 2001; Bian & Zhao 2004; Grupe & Mathur 2004; Mathur & Grupe 2005b,a; Zhou et al. 2006; Schmidt et al. 2016; Rakshit et al. 2017). On the contrary, other authors claimed that NLS1s are *on* the  $M_{BH} - \sigma_*$  relation (Wang & Lu 2001; Botte et al. 2005; Komossa & Xu 2007; Cracco et al. 2016). Sometimes this could be due to the difficulty to directly measure the stellar velocity dispersion in AGNs. To circumvent this, some emission lines such as  $[OIII]\lambda 5007$  or  $[SIII]\lambda 9069$  could be used as a surrogate of  $\sigma_*$  (Nelson & Whittle 1996; Shields et al. 2003; Vega et al. 2009).

Here we re-examine the  $M - \sigma_*$  relation for NLS1s using  $\sigma_*$  directly measured from the Ca II triplet absorption line and the one obtained from stellar synthesis templates. Besides, we tested the use of the “core” of  $[OIII]\lambda 5007$  emission line, after removal of asymmetries, as a replacement for the stellar velocity dispersion.

In this paper we aim to address mainly two issues: (a) to measure the spectral index  $\beta$  in the optical region and the non-stellar contribution to the observed spectra, for a sample of 131 nearby NLS1s taken from the Sloan Digital Sky Survey (SDSS - DR 7) (York et al. 2000; Abazajian et al. 2009), and (b) to study some properties inferred from the emission lines, mainly to revisit the locus of NLS1 galaxies in the  $M - \sigma$  relation found for normal galaxies (e.g., Ferrarese & Merritt 2000; Gebhardt et al. 2000; Tremaine et al. 2002). The sample and data treatment is described in section 2. General results are presented in section 3 and a discussion in section 4. Throughout this paper we assume  $H_0 = 71 \text{ km s}^{-1} \text{ Mpc}^{-1}$ ,  $\Omega_m = 0.3$  and  $\Omega_\Lambda = 0.7$ .

## 2. Data Analysis

### 2.1. Sample selection

Our sample consists of 131 NLS1 at  $z \leq 0.1$  selected from the list of Zhou et al. (2006), also available in the catalogue of Véron-Cetty & Véron (2010). By modelling the emission lines and continua of active objects labelled as “QSOs” or “galaxies” in the SDSS DR3 (Abazajian et al. 2005), Zhou et al. (2006) have performed an exhaustive search and found 2011 NLS1 up to  $z \sim 0.8$ ; this limit corresponds to the detection of  $H\beta$  in SDSS spectral coverage ( $\sim 3800 \text{ \AA}$  to  $9200 \text{ \AA}$ ). We have chosen 131 NLS1 from

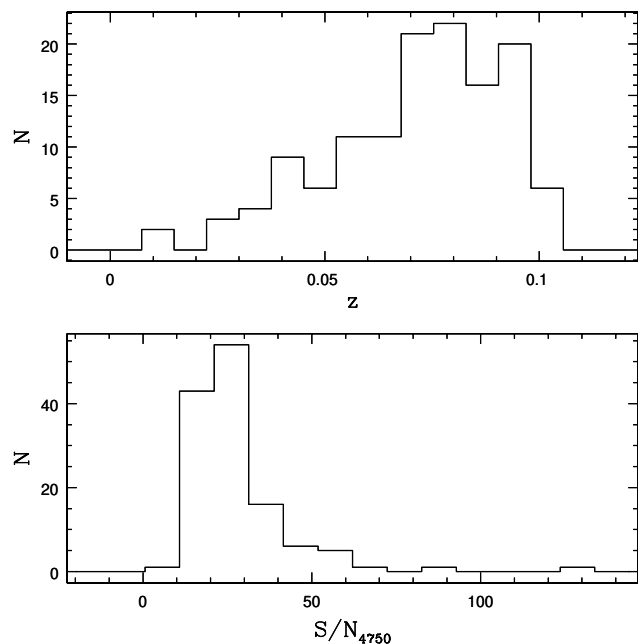


**Fig. 1.** Distributions of the redshift (top panel) and S/N of the continuum measured at rest-frame  $4750 \text{ \AA}$  (bottom panel).

the whole list corresponding to objects nearer than  $z=0.1$  (Fig. 4, top panel). The spectroscopic observations were taken from SDSS DR7, which is complete to a Petrosian magnitude (Petrosian 1976) of 17.77 mag (Strauss et al. 2002). The spectra has a resolution  $\sim 2000$ , and for our sample we measured a mean  $S/N \sim 25$  obtained in the window  $\lambda 4730 - \lambda 4780$  (Fig. 4, middle panel). In the redshift range of our sample, the SDSS fiber aperture of 3 arcsec correspond to  $0.79 - 5.45 \text{ kpc}$  of projected distance, so we are dealing with integrated spectra.

Host galaxy contamination in SDSS spectra can be noticeable even in the case of some quasars (Vanden Berk et al. 2001). After visual inspection of the sample we found that in most cases absorption lines are easily recognised. For instance the CaK  $\lambda 3933$  line is observed in 96 galaxies, while the Na-D lines  $\lambda \lambda 5889.9, 5895.9$  can be seen in 62 cases. The Ca triplet is mostly restricted due to the redshift of the galaxy. Ca II  $\lambda 8498$  was detected in 53 objects, Ca II  $\lambda 8542$  in 59 spectra, while in 23 out of 131 objects the Ca II  $\lambda 8662$  was found. Careful removal of the stellar contribution is essential for proper determinations of the non-stellar continuum as well as for reliable measurements of the recombination emission lines. Besides, this “starlight contamination” provides also valuable information about the host galaxies, which is of interest itself. For this and other purposes, we have developed a technique to properly model the stellar and non-stellar components, which will be explained in the next subsection.

### 2.2. Continuum Modelling

All spectra were corrected for galactic extinction values available in NED (NASA/IPAC Extragalactic Database), calculated according to Schlegel et al. (1998). After extinction correction, we shifted the spectra to rest-frame using redshift values given by SDSS pipelines and re sampled the spectra in steps of  $\Delta\lambda = 1 \text{ \AA}$ . We modelled the continuum of the galaxies using the spec-

tral synthesis code STARLIGHT (Cid Fernandes et al. 2005b; Mateus et al. 2006). This code was widely used to model the stellar populations of SDSS galaxies (Cid Fernandes et al. 2005a), and different samples of AGN (e.g. Cid Fernandes et al. 2004; Bian 2007; Vega et al. 2009; León-Tavares et al. 2011; Benítez et al. 2013). Basically, STARLIGHT models the observed spectrum  $O_\lambda$  to obtain the model  $M_\lambda$  by a linear combination of simple stellar populations (SSPs), as

$$M_\lambda(x, M_{\lambda_0}, A_V, v_\star, \sigma_\star) = M_{\lambda_0} \left[ \sum_{j=1}^N x_j b_{j,\lambda} r_\lambda \right] \otimes G(v_\star, \sigma_\star) \quad (1)$$

where  $b_{j,\lambda} \equiv L_j(\lambda)/L_j(\lambda_0)$  is the  $j$ th SSP normalized at  $\lambda_0$ ,  $x_j$  are the components of the “population vector”,  $M_{\lambda_0}$  is the synthetic flux at  $\lambda_0$ ,  $r_\lambda = 10^{-0.4(A_\lambda - A_{\lambda_0})}$  is the reddening term,  $A_\lambda$  is the internal extinction at  $\lambda$  for each object, which is modelled as a dust screen in the line of sight and parametrized in terms of  $A_V$  (extinction in  $V$ -band) adopting  $R_V = 3.1$  (Cardelli et al. 1989),  $N$  is the total number of components in the spectral base and  $G(v_\star, \sigma_\star)$  is the line of sight stellar velocity distribution modelled as a Gaussian centred at  $v_\star$  with a velocity dispersion  $\sigma_\star$ . The spectra of the base ( $b_{j,\lambda}$ ) are convolved ( $\otimes$ ) in order to take into account the absorption line broadening. The best fit is obtained by means of minimization of  $\chi^2$ ,

$$\chi^2 \equiv \sum_{\lambda_i}^{\lambda_f} [O_\lambda - M_\lambda]^2 \omega_\lambda^2 \quad (2)$$

where  $O_\lambda$  is the observed spectrum,  $\omega_\lambda$  is the weight defined as the inverse of the noise in  $O_\lambda$  and  $\lambda_{i,f}$  are the initial and final wavelengths. Spectral regions that are not wanted to be modelled with STARLIGHT (e.g. emission lines) are masked out by choosing  $\omega_\lambda = 0$ . Besides the high contribution due to the non-stellar continuum and the emission lines, NLS1 spectra often shows some absorption lines, mainly Ca K, Ca H and CaII triplet. These absorption features were given positive weights in the mask (i.e.  $\omega_\lambda > 0$ ), to be sure that the stellar contribution is properly fitted. See Cid Fernandes et al. (2004, 2005b); Mateus et al. (2006) for more details.

When performing this type of analysis it is important to define the base components. To account for the stellar contributions, 80 SSPs of Bruzual & Charlot (2003) were adopted, corresponding to 20 ages and 4 metallicities. The ages are:  $t_\star = 0.00316, 0.00501, 0.00661, 0.00871, 0.01, 0.01445, 0.02512, 0.04, 0.055, 0.10152, 0.1609, 0.28612, 0.5088, 0.90479, 1.27805, 1.434, 2.5, 4.25, 6.25$  and  $7.5 \times 10^9$  years, while the metallicities are  $Z = 0.2, 0.4, 1$  and  $2.5 Z_\odot$ . Besides these stellar components, a power-law (PL) component should be added to the spectral base, since we are dealing with active nuclei. This PL component is usually represented as  $F_\nu \sim \nu^\alpha$  or equivalently  $F_\lambda \sim \lambda^\beta$ , with  $\alpha = -\beta - 2$ . Our contribution to the modelling of the non stellar continuum of NLS1s is the inclusion of a base in the form  $F_\lambda = 10^{20} \times (\lambda/4020)^\beta$ , corresponding to 6 spectral indexes  $\beta$  ranging from  $-3$  to  $-0.5$ , with steps of  $0.5$ . As discussed in Cid Fernandes et al. (2004) noise in the spectra dilutes the differences in the base components which are similar due to intrinsic degeneracies. A way to avoid this is by grouping the  $x_j$  of similar spectral components, which would return a more reliable result. Thus, the fraction of the observed flux due to the power-law component can be parametrized as:

$$F_{PL} \sim \sum_{i=1}^6 X_{PL_i} \lambda^{\beta_i} \quad (3)$$

from which we can derive a single power-law with a mean spectral index  $\langle \beta \rangle$  for each galaxy. We do not seek to assign any physical meaning to this PL base component, since it is merely included to add a free parameter to the fit.

This method allow us to identify three important parts of an AGN spectrum: the stellar populations, the non-stellar continuum and the difference between the total flux and the sum of this two components, giving us the residual spectra, i.e. the ionized interstellar gas. The search for the stellar and non-stellar contributions is made by computing equation 2 for each galaxy, after masking the emission lines. We show in Figure 2 examples of spectral synthesis for selected galaxies. In this figure the observed spectrum is shown in thick solid line, the modelled spectrum in thin line, the contribution due to the mean spectral index is in dots, and the residual spectra in the bottom panel. An estimate of the errors in the parameters acquired from STARLIGHT were obtained using the jackknife technique. For this, we run the code 85 times, taking away one component of the base in each run. The adopted error was the dispersion (at  $1 \sigma$ ) in the distribution of the measurement of each parameter. From this we have a typical uncertainty of  $\pm 0.2$  for  $\beta$  and of  $\sim 5\%$  for  $F_{PL}$ . For those objects with contribution of  $F_{PL}$  less than  $\sim 50\%$  the uncertainties in these parameters were larger.

### 2.3. Absorption lines

As mentioned before, a significant portion of our sample presented absorption lines in their observed spectra. We chose to measure the Ionized Calcium K and Calcium triplet lines for being the stellar features with highest S/N and less contamination due to emission lines or non-stellar continuum. In the case of Ca II triplet (CaT), we used the Penalized Pixel-Fitting method (pPXF) Cappellari (2017) to extract the stellar kinematics. We fit the kinematics of the CaT using MILES stellar library (Vazdekis et al. 2016), in the range 8350–9020Å with a resolution of  $1.5\text{Å}$ (FWHM). On the other hand, Ca K absorption line was measured using the FITPROFS task included in IRAF<sup>1</sup>, assuming that a single Gaussian function was sufficient to fit the profile. All FWHM were corrected for instrumental broadening ( $\text{FWHM}_{inst}$ ) considering the resolution given by Sloan of  $\text{FWHM} = 2.7 \text{Å}$  at  $\lambda = 4861$ . In Fig. 3 we show examples of spectra with prominent absorption lines, and in Fig. 4 (bottom panel) we show the equivalent width (EW) distribution for the CaK and CaII $\lambda$ 8542 lines. The EW of CaK has a mean value of  $2.8 \pm 1.9$  and median of 2.6 with an IQR of 2.5, while the EW of CaII $\lambda$ 8542 has a mean value of  $2.2 \pm 0.9$  and a median of 2.2 with an IQR of 1.3.

### 2.4. Iron emission lines

The primary challenge in measuring accurate fluxes of emission lines (see sec. 2.5) is to properly subtract any kind of contamination. NLS1s usually show strong optical FeII emission lines (e.g., Véron-Cetty et al. 2004; Zhou et al. 2006; Cracco et al. 2016) and some authors even suggest to adopt the flux ratio of FeII to H $\beta$  as a better parameter to differentiate them from BLS1s (Véron-Cetty et al. 2001). We focused part of our analysis in

<sup>1</sup> IRAF: the Image Reduction and Analysis Facility is distributed by the National Optical Astronomy Observatories, which is operated by the Association of Universities for Research in Astronomy, Inc. (AURA) under cooperative agreement with the National Science Foundation (NSF) Tody (1993).

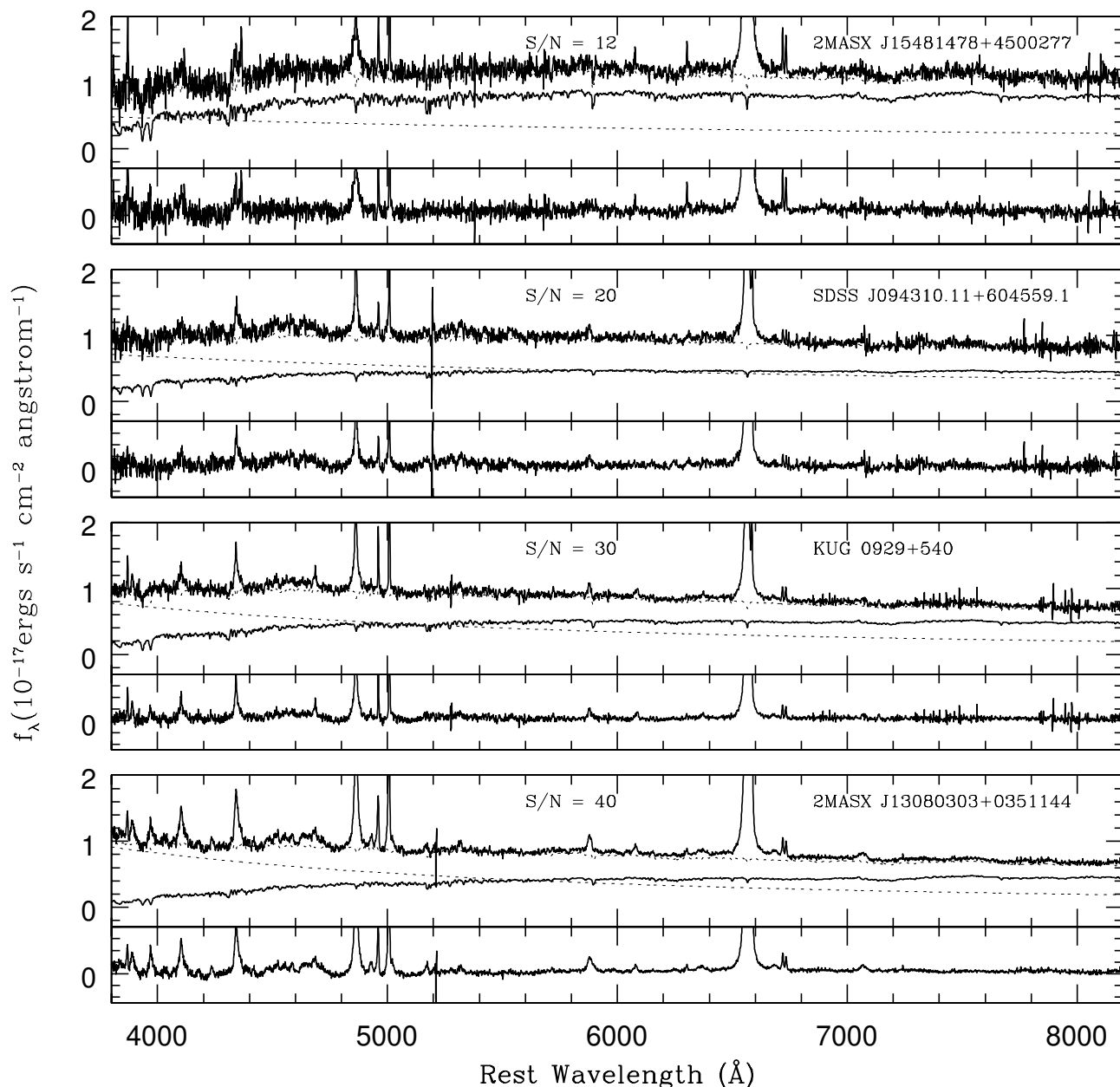


**Fig. 2.** Representative examples of spectral fitting. In each panel, we plot the observed spectrum (thick solid line), the modelled spectrum (dotted), the host galaxy spectrum (thin solid line), the power-law contribution (dotted), and the residual spectra (lower panel). The observed spectra is normalized at the flux value in  $\lambda = 4020$ .

the spectral emission lines on the  $H\beta$  region, between 4000 and 5500Å, where strong FeII multiplets are often present. We subtracted the iron emission lines using the online software developed by Kovačević et al. (2010) and Shapovalova et al. (2012)<sup>2</sup>. This software provides a best-fit model that reproduces the iron multiplets in the  $H\beta$  region for each object in function of the gas temperature, Doppler broadening, and shift of the FeII lines. The software performs a  $\chi^2$  minimization routine to obtain the best fit. To fit each line, it assumes that it can be represented by a Gaussian, described by width, shift, and intensity. Given that

these lines are likely to be originated in the same region, with the same kinematical properties, values of shift and width are assumed to be the same for all Fe II lines in the case of one AGN. See Fig. 5 for an example.

### 2.5. Line measurements

After subtraction of the stellar and non-stellar components and the Fe multiplets, we are left with the lines emitted by the ionized gas. Emission line profile fitting have been tackled in different ways by various authors. For low line-of-sight inclination

<sup>2</sup> [http://servo.aob.rs/FeII\\_AGN/](http://servo.aob.rs/FeII_AGN/)

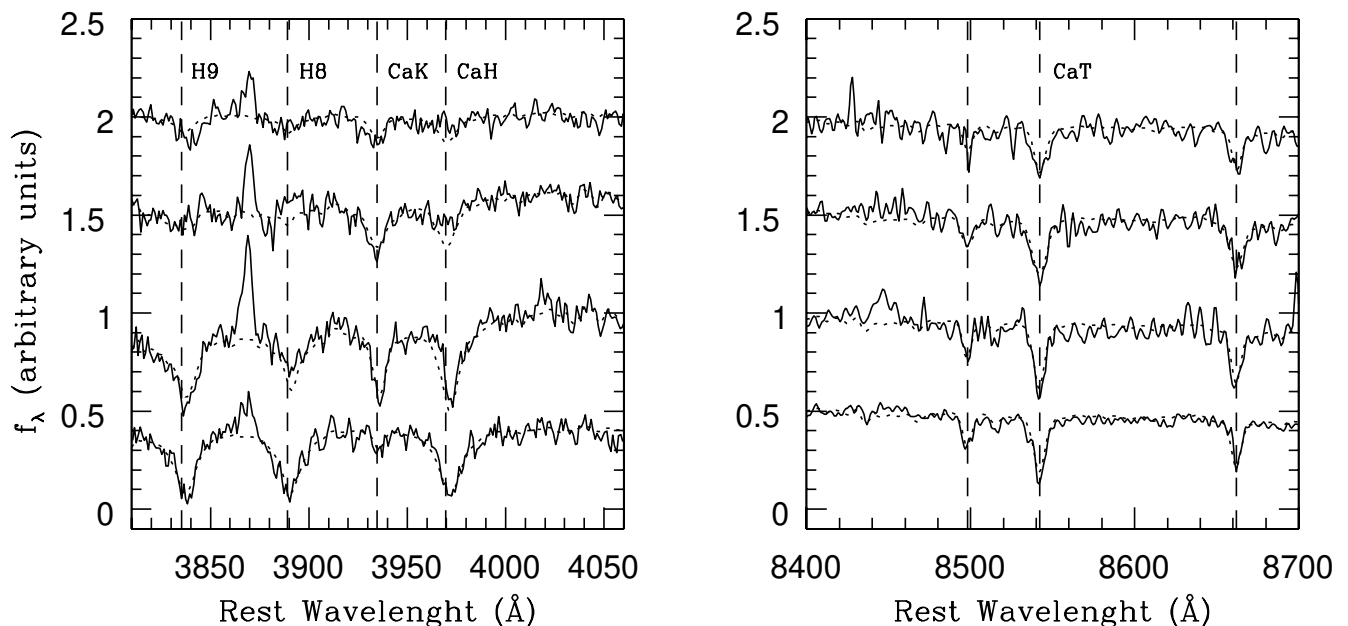


**Fig. 3.** Example of NLS1 galaxies with noticeable absorption lines. Represented in solid line is the observed continuum and in dotted line the synthetic spectra obtained with STARLIGHT.

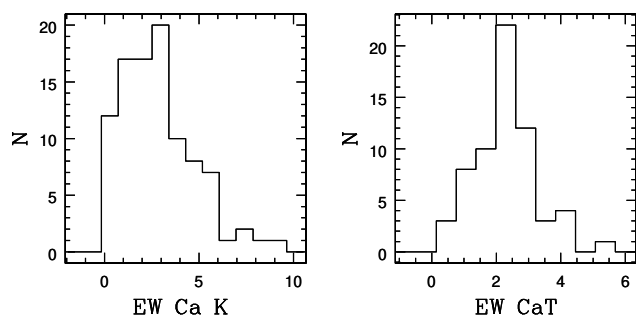


**Fig. 4.** Distributions of the equivalent width of the CaK line (left) and CaII $\lambda$ 8542 line (right) for our sample.

systems [Goad et al. \(2012\)](#) concludes that turbulence dominates over the planar Keplerian motion resulting in Lorentzian profiles for lines formed at large BLR radii. From observational studies of NLS1 spectra, in order to model the broad component of H $\beta$  some authors chose the Lorentz profile (e.g., [Zhou et al. 2006](#); [Cracco et al. 2016](#); [Rakshit et al. 2017](#)). On the other hand, some authors suggest that a multiple Gaussian profile fitting yields a more statistically robust result than the Lorentzian component fitting method ([Dietrich et al. 2005](#); [Mullaney & Ward 2008](#)). We assumed in our analysis that the emission line profile of the broad component of H $\beta$  in NLS1 galaxies can be represented by a single or a combination of Gaussian profiles (e.g., [Scharwächter et al. 2017](#); [Schmidt et al. 2016](#); [Mullaney & Ward 2008](#); [Schmidt 2019](#)). For this purpose we used the LINER routine ([Pogge & Owen 1993](#)), which is a  $\chi^2$  minimization algorithm that can fit several Gaussians to a line profile. We fitted the [OIII]  $\lambda$ 4959 and  $\lambda$ 5007 lines with one Gaussian for the core component, and one or two additional Gaussian components for the asymmetric emission profiles, depending on the case (e.g.,

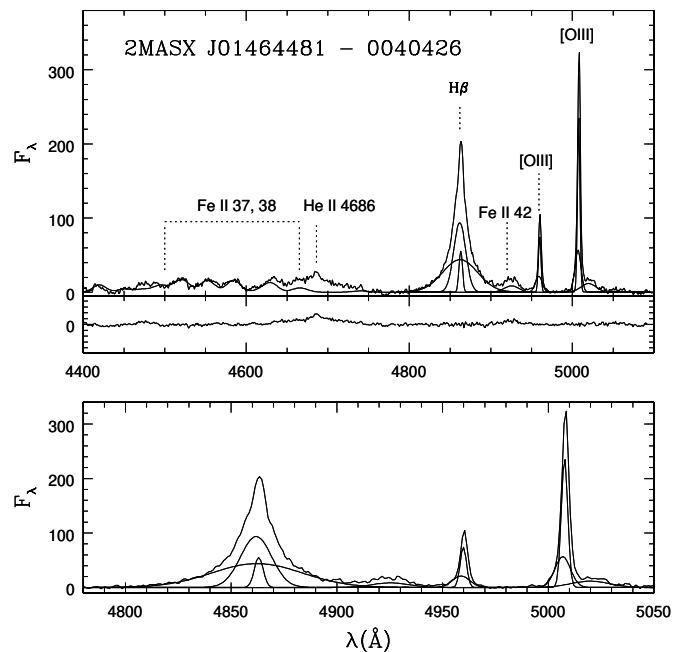


**Fig. 5.** Top panel shows the Gaussian decomposition and iron fit for the galaxy 2MASX J01464481-0040426. The observed spectrum flux is in arbitrary units (thick line); FeII template and Gaussian components obtained with LINER are in thin lines. The residual spectra is plotted on the lower sub-panel for clarity. The bottom panel shows a zoomed view of the H $\beta$ + [OIII] observed spectrum and its fit.

[Cracco et al. 2016](#)). In our sample, 28 galaxies showed no asymmetries and were fitted with only one component, 86 galaxies were fitted with one extra Gaussian for the asymmetric emission, while 15 galaxies needed the inclusion of 2 extra components. In a similar way we also fitted H $\beta$ , which is one of the strongest per-

mitted lines in the optical range. We fitted the narrow component taking into account that it should have approximately the same FWHM than the core component of [OIII] $\lambda$ 5007 (Schmidt et al. 2018) and one or two Gaussian components to fit the broad emission as mentioned. Two galaxies (SDSS J144249.70+611137.8 and SDSS J103210.15+065205.3) show no emission in H $\beta$  and therefore they were excluded from the subsequent analysis. In order to assess the measurement uncertainties, we measured the emission lines at least 15 times in galaxies with different S/N. In the case of a galaxy with a S/N of  $\sim 13$ , we found a relative error in the measured values of  $\sim 20\%$  for the FWHM and of  $\sim 4\%$  for the flux of the narrow component of H $\beta$  and 1% and 3% for the FWHM and flux errors of the broad component of H $\beta$ . For the [OIII] lines, the uncertainties are of the order of  $\sim 4\%$  and 9% for the FWHM and flux measurements of the central component, and of 30% and 20% for the FWHM and flux of the asymmetric component. Considering galaxies with a typical S/N ( $\sim 26$ ), the measurement errors are of 4% for the FWHM and flux of the narrow component of H $\beta$ , and of 10% and 20% for the FWHM and flux of the broad component of H $\beta$ . In the case of [OIII] line, the relative errors are of the order of 5% and 10% FWHM and flux respectively, in the case of the core component and 10% and 2% for the FWHM and flux of the asymmetric component. A typical fit is shown in 5.

### 3. Results

#### 3.1. Non-Stellar content in AGNs

Here we are mainly focused on the non-stellar continuum of AGN, which were calculated using a spectral base of power-law, as described in section 2.2. We stress that, unlike other works, we obtain simultaneously the non-stellar contributions  $F_{PL}$  and the optical slopes for each AGN. This technique differs from what is accepted by other authors, for instance, always assuming the same spectral index (e.g., Zhou et al. 2006) or by taking all the observed continuum as arising from the active nucleus, as may occur in quasars and Seyfert 1s (e.g., Greene & Ho 2005; Pu et al. 2006; Vanden Berk et al. 2001). In other works such as Barth et al. (2015) they modelled the non-stellar continuum as a power-law with free parameters, but they use a single 11 Gyr, solar metallicity, single-burst spectrum from Bruzual & Charlot (2003) to model the host galaxy contribution. For our sample we set free in the code the stellar and non-stellar contributions, without prior over the steepness neither the fraction of power-law or the stellar populations. The results are shown in Figure 6. We found that the values of  $\beta$  ranges between  $-2.9$  and  $0$  with a mean value of  $\beta = -1.6 \pm 0.6$  and a median of  $-1.6$  with an IQR =  $0.9$ , while for the contributions of the non-stellar component (right panel) we found a mean value of  $F_{PL} = 0.61 \pm 0.22$  and a median of  $0.64$  with IQR =  $0.29$ , in concordance with Zhou et al. (2006). Contrary to what we expected, we did not find any correlation between  $\beta$  and  $F_{PL}$  with a Pearson correlation value of  $r = 0.11$ ,  $p$ -value =  $0.24$ .

We checked our method applying it to a sample of galaxies with low contribution from the AGN (as in the case of Seyfert 2) and another sample with a high AGN contribution to the observed continuum (QSO). We constructed the sample of Seyfert 2 galaxies by taking 200 galaxies from the Véron-Cetty & Véron (2010) catalogued as Seyfert 2 randomly selected in the redshift range  $0.01 < z < 0.1$ . For the QSO sample, we selected 100 QSO defined as isolated in the redshift range  $0.2 < z < 0.31$  from

Donoso et al. (2018). For the sample of Seyfert 2 galaxies we obtained a  $F_{PL}$  with a median of  $0.19$  and IQR of  $0.06$ . This is in agreement with previously found results (Cid Fernandes et al. 1998; Schmitt et al. 1999; Cid Fernandes et al. 2004). In the case of the QSO sample, the median value of  $F_{PL}$  measured was of  $0.92$  with an IQR of  $0.30$ , in concordance with previous results (Vanden Berk et al. 2006; Lyu et al. 2016; Lani et al. 2017). The results obtained for the  $F_{PL}$  of these comparison samples are shown in Figure 6, right panel.

Some spectral properties can be more evident in combined spectra of objects of the same class, as was pointed out by Vanden Berk et al. (2001). Combining the spectra can also be a useful tool often used to increase the S/N ratio. Such composites have been studied in several occasions for quasars and BLAGNs (Francis et al. 2001; Wilhite et al. 2005; Pol & Wadadekar 2017) to study the shape and variability of the continuum. We performed a stacking of the 131 spectra taking the geometrical mean value of the flux. As mentioned in Vanden Berk et al. (2001), the statistical method used to combine the spectra will preserve different quantities. In this context, the geometric mean preserves the shape of the continuum. We performed spectral synthesis on the geometric stacked spectra and through equation 3 we obtain a mean value of  $\beta_{(geo)} = -1.55$  with  $F_{PL (geo)} = 0.63$ . The stacked spectra and model can be seen in Figure 7.

#### 3.2. Emission Lines

Besides their characteristic continua, NLS1 exhibit some emission features that deserves attention. These include strong permitted Fe II emission lines in their optical and ultraviolet spectra, asymmetric [OIII] lines, and multiple component H $\beta$  profile (e.g., Mullaney & Ward 2008; Schmidt et al. 2018). The relative strength of the FeII multiplets is conventionally expressed as the flux ratio of FeII to H $\beta$ :  $R_{4570} \equiv \text{Fe II } \lambda\lambda 4434 - 4684 / \text{H}\beta$ , where FeII $\lambda\lambda 4434 - 4684$  denotes the flux of the FeII multiplets integrated over the wavelength range of  $4434 - 4684\text{\AA}$ , and H $\beta$  denotes the total flux of H $\beta$  (e.g. Xu et al. 2012; Cracco et al. 2016). We found that  $R_{4570}$  ranges between  $0.15 - 2$ , with a median of  $0.74$  with an IQR of  $0.42$ . This value is higher than  $R_{4570} \sim 0.49$  found by Cracco et al. (2016). Nonetheless, our measurements are consistent with those of Zhou et al. (2006) and Xu et al. (2007, 2012), who found average values of  $0.82$ ,  $0.75$  and  $0.7$  respectively.

We explored if there is a connection between the iron emission and the shape of the non-stellar continuum ( $\beta$ ). We find no correlation between the  $F_{PL}$  and  $R_{4570}$ , with a Pearson coefficient of  $r = -0.17$  and  $p$ -value =  $0.095$ . A mild correlation is found between the shape of the non-stellar continuum ( $\beta$ ) and  $R_{4570}$ , with  $r = 0.36$ ,  $p$ -value =  $0.0003$ . This would contribute to the hypothesis that photoionization is not the only mechanism involved in the FeII emission (Rodríguez-Ardila et al. 2000; Cracco et al. 2016).

We show in Figure 8 the FWHM distribution for the broad and narrow component of H $\beta$ . Left panel shows the broad component of H $\beta$  with values ranging between  $\sim 900 - 4500 \text{ km s}^{-1}$  and a median value of  $2280 \text{ km s}^{-1}$  and IQR =  $1857 \text{ km s}^{-1}$ . The differences in FWHM from the measured by Zhou et al. (2006) seem to be mainly due to the different criteria adopted to fit the broad component of H $\beta$ . However, we chose not to discard any of the galaxies with FWHM  $> 2000 \text{ km s}^{-1}$  considering that AGN with FWHM H $\beta \leq 4000 \text{ km s}^{-1}$  belong to the same population (Sulentic et al. 2000; Marziani et al. 2018). Most

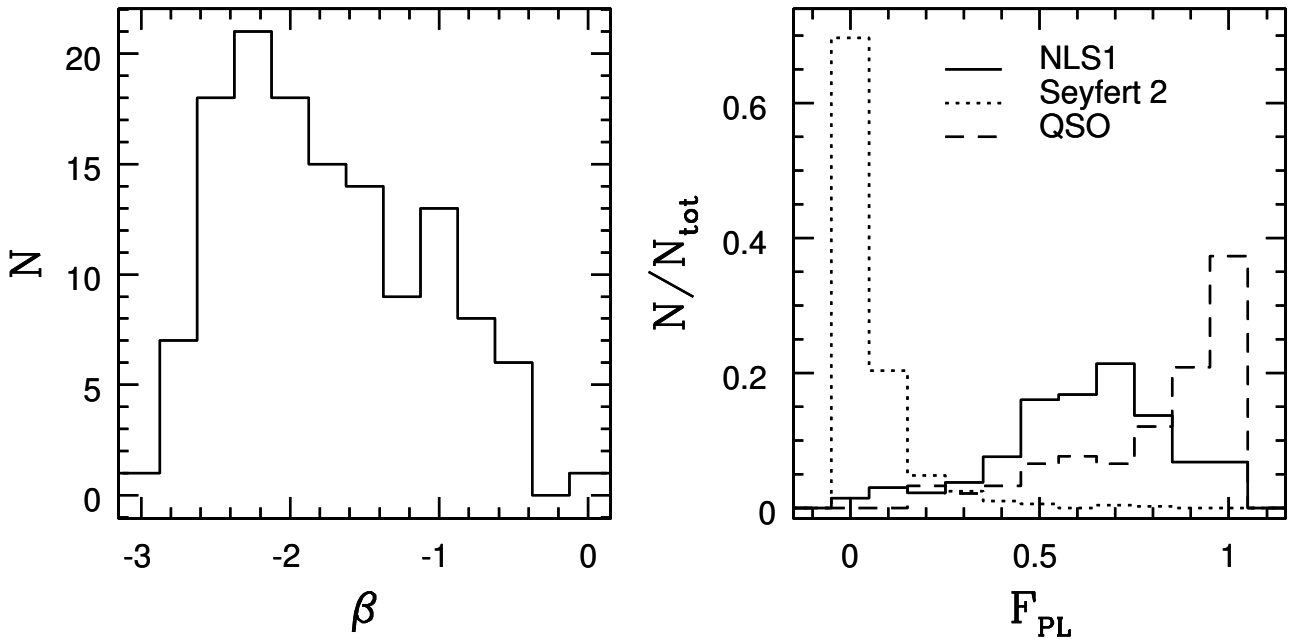


**Fig. 6.** Distribution of power-law indexes obtained from STARLIGHT for our sample of 131 NLS1 (left panel) and fraction of contribution of this component to the total spectra (right panel). Solid line represents NLS1, dotted line BLAGNs and dashed line Seyfert 2 galaxies.

galaxies present a narrow component FWHM from 0 to  $\sim 800$   $\text{km s}^{-1}$ , with a median of  $257$   $\text{km s}^{-1}$  and  $\text{IQR} = 174$   $\text{km s}^{-1}$ . As mentioned before, two galaxies lack  $\text{H}\beta$  in emission and we also found three "outliers" with values above  $800$   $\text{km s}^{-1}$ . They are 2MASX J22545221+0046316, SBS 0933+511 and 2MASX J08183571+2850224 with FWHM of  $\text{H}\beta$  of 890, 950 and 1390  $\text{km s}^{-1}$  respectively.

We derived the luminosity  $\lambda L_{\lambda}(5100)$  from the flux of the featureless continuum given by the power-law component and studied the relation between the strength of the AGN ( $\lambda L_{\lambda}(5100)$ ) and the luminosity of the Balmer emission line  $\text{H}\beta$ . As expected for sources with emission dominated by photoionization, a strong correlation was found between the luminosity of the broad component of  $\text{H}\beta$  and  $\lambda L_{\lambda}(5100)$ , with a Pearson correlation coefficient  $r=0.91$  and  $p=3.4\text{e-}48$ , being this result in excellent agreement with Zhou et al. (2006); Cracco et al. (2016). Considering the narrow component of  $\text{H}\beta$ , it follows the same trend although with a smaller but still significant correlation coefficient of  $r=0.66$  and  $p=2.6\text{e-}17$  (right panel of Figure 9).

### 3.3. Black Hole Masses and nuclear properties

Supermassive Black Holes are of crucial interest in the study of AGNs. Determining their properties leads to the understanding of many mechanisms involved in the innermost regions of active galaxies. Several lines of evidence hint at small black hole masses ( $M_{BH}$ ) as well as to high accretion rates in NLS1 galaxies (e.g., Mathur et al. 2001; Nikolajuk et al. 2009; Woo et al. 2015). According to Greene & Ho (2005),  $M_{BH}$  can be estimated through luminosity and FWHM of the broad component of  $\text{H}\beta$ , as follows:

$$M_{BH} = 3.26 \times 10^6 \left( \frac{L_{H\beta}}{10^{42} \text{erg s}^{-1}} \right)^{0.56} \left( \frac{FWHM_{H\beta}}{10^3 \text{km s}^{-1}} \right)^2 M_{\odot} \quad (4)$$

This relation is very useful as involves the luminosity and FWHM of the same Balmer emission line which are easily detectable even in distant AGNs. We determined  $M_{BH}$  of the sample using equation 4 taking into account the broad component of  $\text{H}\beta$ , after correcting for instrumental resolution. Since the errors in the measurements of the luminosity and FWHM are typically of 15% and 10% respectively, the error propagation for  $M_{BH}$  gives an uncertainty of  $\sim 0.1$  dex. In our sample, almost all of the galaxies have  $M_{BH}$  spanning the values between  $\log(M_{BH}/M_{\odot}) = 5.6 - 7.5$ , with a mean value in  $\log(M_{BH}/M_{\odot}) = 6.5 \pm 0.4$  and a median value of 6.5 with  $\text{IQR} = 0.6$ . This is in agreement with previous results (e.g., Grupe & Mathur 2004; Zhou et al. 2006; Komossa & Xu 2007; Schmidt et al. 2016; Cracco et al. 2016).

It has been demonstrated that  $M_{BH}$  is tightly correlated with the stellar velocity dispersion of the bulge of normal galaxies,  $\sigma_{\star}$  (Ferrarese & Merritt 2000; Gebhardt et al. 2000). Nelson et al. (2004) measured the bulge stellar velocity dispersion in 14 Seyfert 1 galaxies whose  $M_{BH}$  were determined using the reverberation mapping technique and showed that the Seyfert galaxies followed the same  $M_{BH} - \sigma_{\star}$  relation as non-active galaxies. Different studies of NLS1 galaxies have conflicting results about their location on the  $M_{BH} - \sigma_{\star}$  relation. One of the goals of this work is to re examine this relation using different methods to estimate  $\sigma_{\star}$ . It is important to note that for AGNs the stellar lines are usually diluted by the strong non-stellar continuum, and NLS1 are not an exception to that. Nonetheless, some absorption spectral features are evident in their spectra, since we can detect stellar features like CaH+K, Mg and CaT lines, after careful inspection of the data (see sec. 2.1). We obtained an estimation of  $\sigma_{\star}$  directly through spectral synthesis technique by means of the code STARLIGHT. This code performs a fit over all the stellar features and provides a  $V_d$  parameter, which is actually a mean broadening parameter applied to the model which best fits the data. To get the proper  $\sigma_{\star}$  we must correct this value from the instrumental and base spectral resolution as:  $\sigma_{\star}^2 = V_d^2 - \sigma_{inst}^2 + \sigma_{base}^2$ . We adopted the spectral

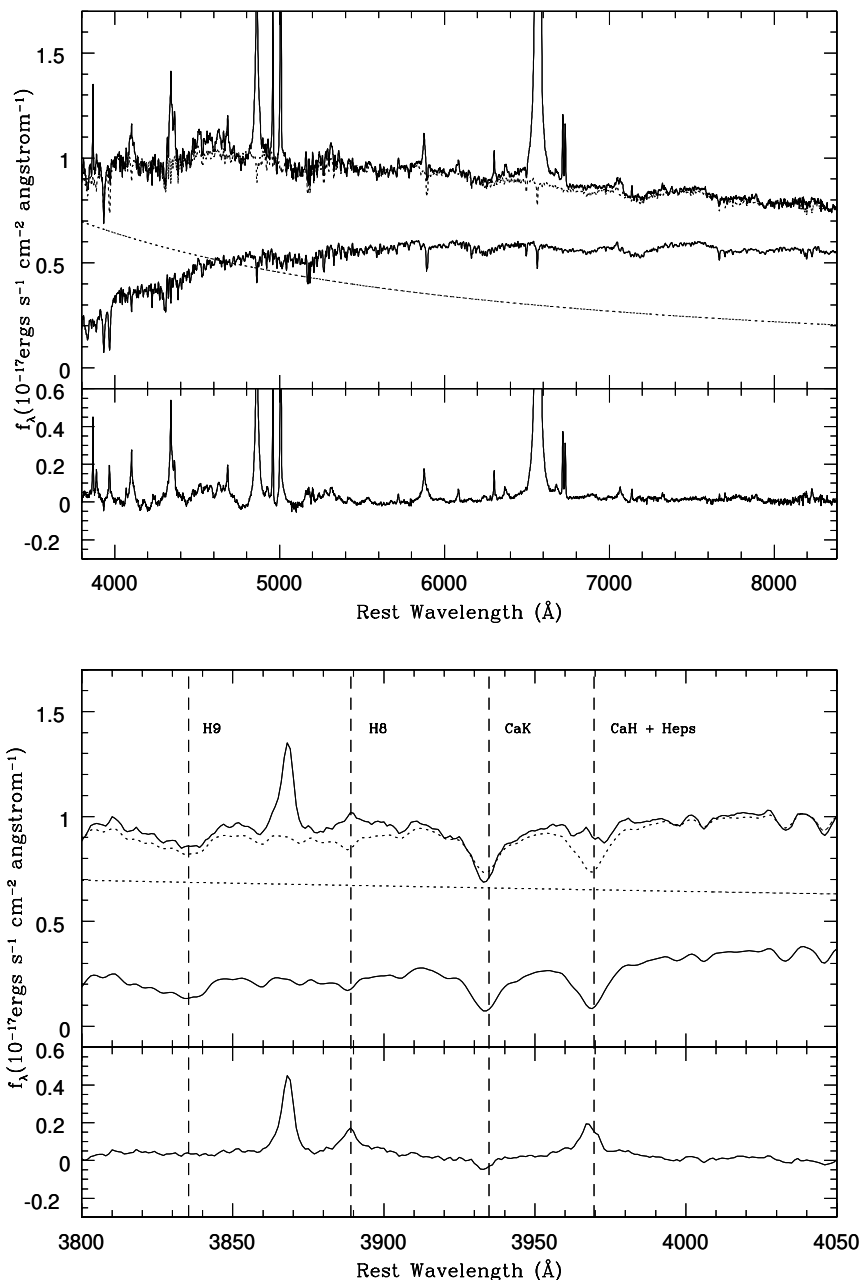


**Fig. 7.** Top panel shows the stacked spectra with geometric mean, bottom panel shows the arithmetic mean. We plot as in Figure 2 the observed spectrum (thick solid line), the modelled spectrum (dotted), the host galaxy spectrum (thin solid line), the power-law contribution (dotted), and the residual spectra (lower panel). The observed spectra is normalized at the flux value in  $\lambda = 4020$ . Bottom: same as top panel, zoomed in the blue part of the spectra.

resolution given by SDSS of  $\sigma_{inst} \sim 68 \text{ km s}^{-1}$  in the vicinity of  $\lambda = 5000 \text{ \AA}$  and for the base spectra (extracted from Bruzual & Charlot 2003)  $\sigma_{base} \sim 76 \text{ km s}^{-1}$  at the same wavelength.

Although the region  $7500 \text{ \AA} - 9000 \text{ \AA}$  is affected by sky contamination, SDSS spectra residuals are similar in this range and in the Ca H+K vicinity. Besides the AGN contribution is less powerful in the red region of the spectra, so the CaT lines will be less diluted than the absorption lines in the blue region. In this scenario, Greene & Ho (2006) argue that Ca triplet lines (CaT in  $8498 \text{ \AA}$ ,  $8542 \text{ \AA}$  and  $8662 \text{ \AA}$ ), provides the most reliable measurements of  $\sigma_*$  in AGNs. Furthermore, the width of the [OIII] $\lambda 5007$  emis-

sion line is often used instead of stellar velocity dispersion due to observational difficulty of the latter. As stressed by Komossa & Xu (2007) the width of [OIII] $\lambda 5007$  line is a good surrogate for the stellar velocity dispersion, when only the core of the line is considered, (the same situation holds for the NIR [SIII] $\lambda 9069$ ; Vega et al. 2009).

In Figure 10 it can be seen the locus of NLS1 in the  $M_{BH} - \sigma_*$  relation, with  $\sigma_*$  obtained from these different approach previously mentioned. To ensure a proper spectral decomposition we considered only those galaxies with broad component of H $\beta$ , at least one CaT absorption line detected, and a narrow component of [OIII] $\lambda 5007$  reliably measured. 67 galaxies in our sample



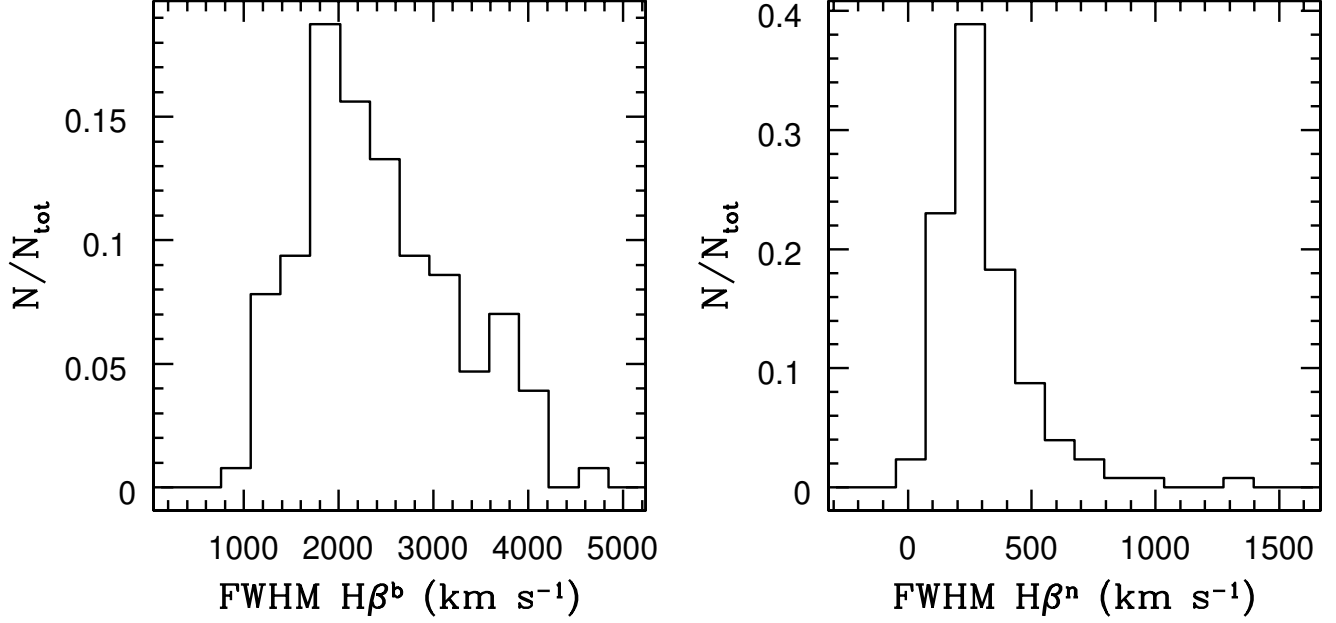


**Fig. 8.** FWHM distribution for the broad (left) and narrow (left) component of  $H\beta$ . Units are in  $\text{km s}^{-1}$  and were corrected by instrumental broadening.

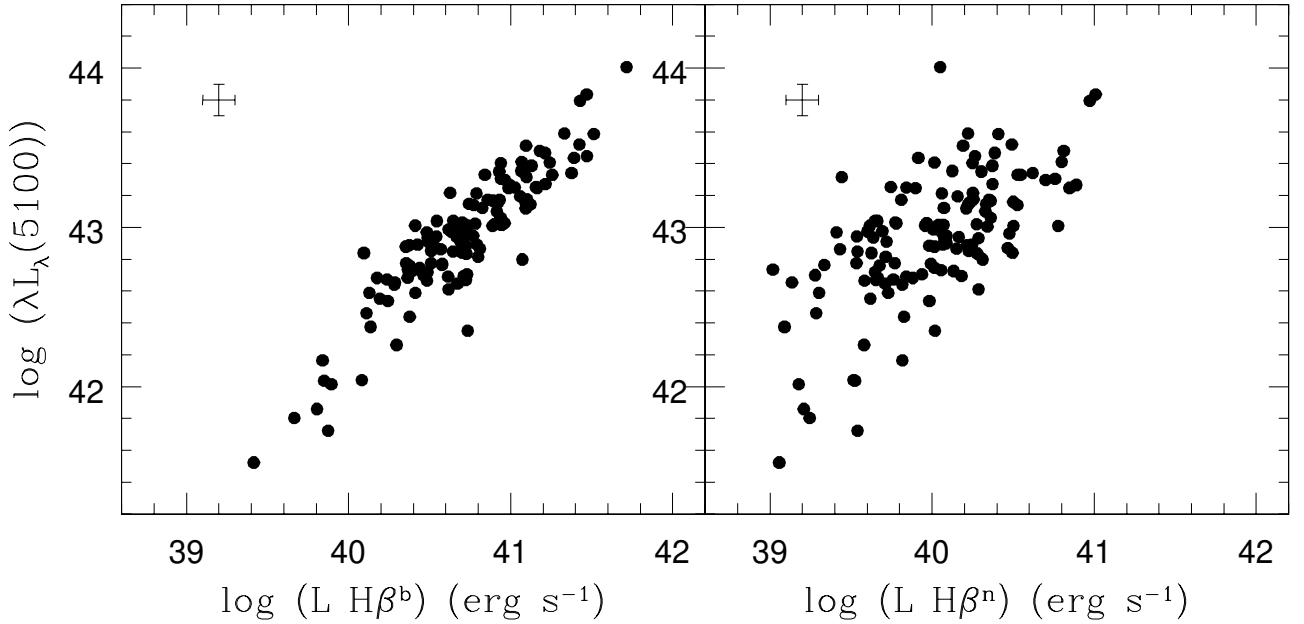


**Fig. 9.** Luminosity of the featureless continuum in  $\lambda=5100$  against the luminosity of the broad (left) and narrow (right) component of  $H\beta$ .

complies with these three constrains simultaneously. The well-known  $M_{BH} - \sigma_*$  relation for normal galaxies, as parametrized by Tremaine et al. (2002),

$$\log\left(\frac{M_{BH}}{M_\odot}\right) = (8.13 \pm 0.06) + (4.02 \pm 0.32)\log\left(\frac{\sigma_*}{200\text{km s}^{-1}}\right) \quad (5)$$

is marked in the plots by the solid line. It can be seen that NLS1 galaxies seem to follow the  $M_{BH} - \sigma_*$  relation when the stellar velocity dispersion estimated from CaT lines and from STARLIGHT are considered (left and central panel in Figure 10). Taking into account the velocity dispersion of the gas emitted from the NLR, given by the FWHM of the core component of  $[OIII]\lambda5007$ , this relation still holds.

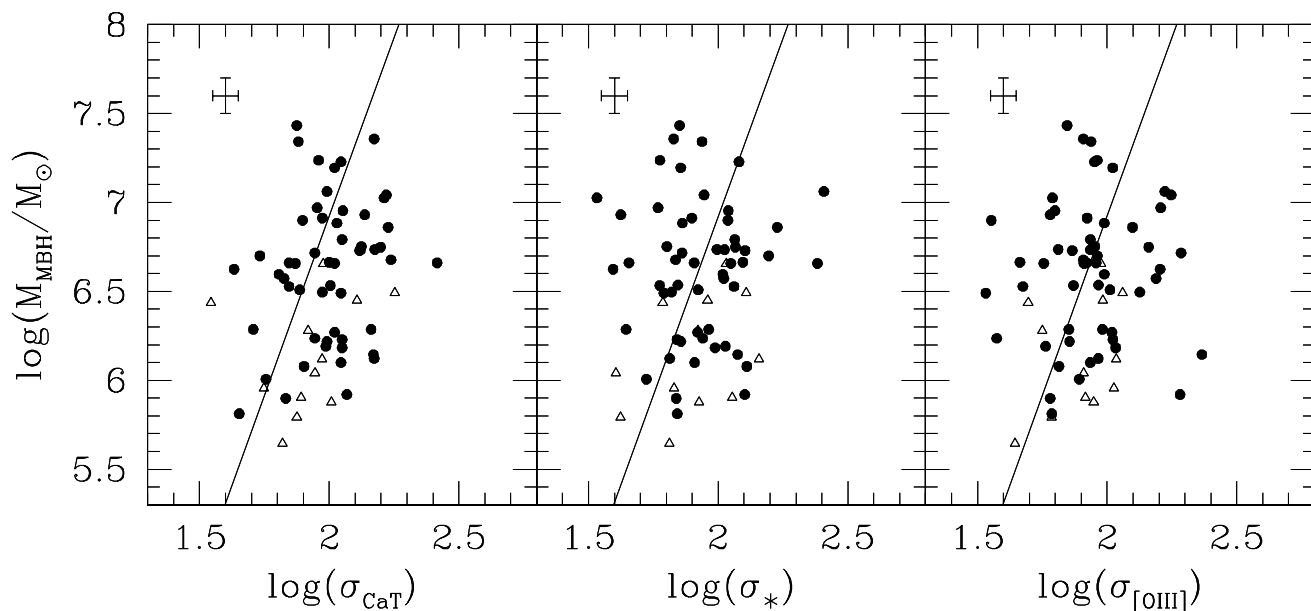


**Fig. 10.** Relation between the black hole mass and the stellar velocity dispersion measured from the Calcium triplet ( $\sigma_{CaT}$ ),  $\sigma_*$  obtained from STARLIGHT and  $\sigma_{[OIII]}$  from the core component of [OIII] $\lambda$ 5007. Open triangles represent galaxies with  $L_{bol}/L_{Edd} > 1$  and the solid line represents the relation given by Tremaine et al. (2002) for normal galaxies.

Closely linked to black hole masses is the accretion rate relative to the Eddington rate, generally parametrized as ratio of  $L_{bol}/L_{Edd}$ , where the bolometric luminosity correction was assumed as  $L_{bol} \sim 3500 \times L_{[OIII]}$  (Heckman et al. 2004), and  $L_{Edd} = 1.26 \times 10^{38} M_{BH}/M_{\odot} \text{ergs}^{-1}$ . We found that several objects in our sample accrete close to or at higher rates than the Eddington luminosity. Also an anti-correlation between the accretion rate and the black hole mass is observed ( $r = -0.59$  and  $p\text{-value} = 1.1 \times 10^{-10}$ ), indicating that lower mass black holes are growing faster than more massive ones, as shown in Figure 11.

We compared the BH masses of our sample and  $F_{PL}$  of their total emission and we found an interesting correlation between them, with a Pearson coefficient of  $r = 0.59$  and  $p\text{-value} = 1.7 \times 10^{-13}$ . In Figure 12 it can be seen that, in general, objects with lower BH masses have lower  $F_{PL}$  while galaxies with  $F_{PL} > 50\%$  have BH masses  $\log(M_{BH}/M_{\odot}) > 7$  in the high end of the relation. It has been well established the relation between the continuum luminosity and the central black hole mass (Kaspi et al. 2000; McLure & Dunlop 2002; Vestergaard 2002), with higher luminosities at greater BH mass. From our results we obtain that the host galaxy contribution to the observed total spectra, decreases at higher BH masses, i.e., the continuum luminosity complete dilutes the stellar features of the spectrum.

#### 4. Discussion

The shape and strength of the continuum in NLS1 spectra is still a matter open for debate. Typically, the AGN continuum spectra are modelled as power-laws, with the slope of the continuum assumed to be the same for all classes of AGNs. We found a large degeneracy for  $\beta$  when the contribution of the non-stellar continuum is less than  $\sim 40\%$ . The errors in the determination of the slope grow significantly when the power-law contribution is minor. Studying a sample of 7 NLS1 galaxies using optical

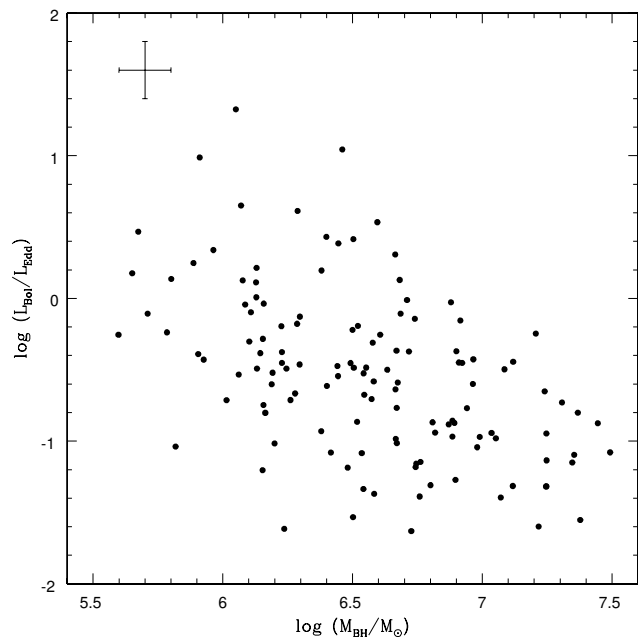


**Fig. 11.** Accretion rate relative to the Eddington Luminosity versus Black Hole Mass

and near-IR CCD spectroscopy Rodríguez-Ardila et al. (2000) found an average value of  $\beta = -1.41$ , while Cracco et al. (2016) found a mean value of  $\beta = -1.22$  for a sample of 296 NLS1. Several works have computed the value for the spectral slope in AGN in the optical range from composite spectrum, such as Francis (1996); Vanden Berk et al. (2001) who found mean val-

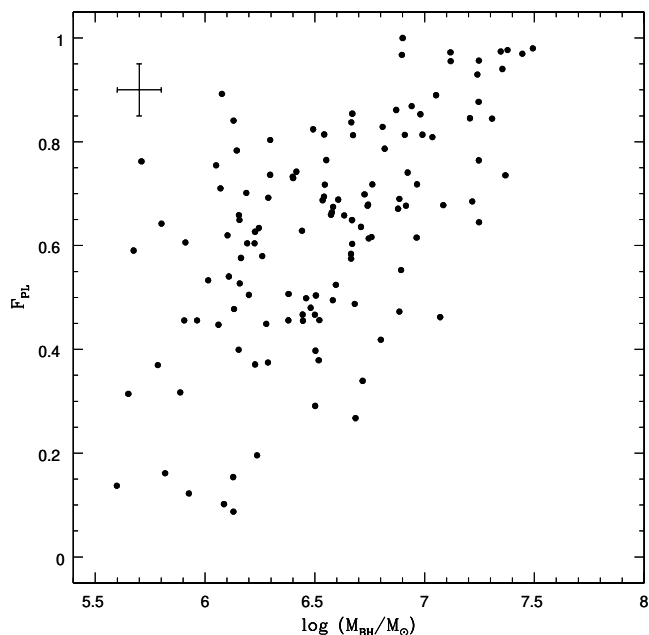


**Fig. 12.** Fraction of power-law contribution versus Black hole mass.

ues for  $\beta$  of  $-1.65$  and  $-1.55$  respectively, from samples of QSO. [Pol & Wadadekar \(2017\)](#) found a value of  $-1.89$  from Seyfert 1 composite spectra, and they argued that the difference in the steepness of the spectra in wavelengths redder than  $4000\text{\AA}$  is due to an increase in the contribution to the flux from the host galaxy. When we consider the contribution to the spectra by the featureless continuum  $F_{PL}$  is evident that the host galaxy has a non-negligible impact in the observed spectra, and that NLS1 galaxies are an intermediate case between QSO and Seyfert 2 galaxies (see Figure 6).

The well know relations between the central black hole and their host galaxy are a key role to understand the black hole formation and evolution. Multiple evidence points toward a correlation between the  $M_{BH}$  and the mass of the bulge (e.g., [Kormendy & Richstone 1995](#); [Magorrian et al. 1998](#)) and also with the stellar velocity dispersion (e.g., [Ferrarese & Merritt 2000](#); [Kormendy & Ho 2013](#)), suggesting that the velocity dispersion is an important parameter to understand  $M_{BH}$  evolution. As mentioned in sec. 1, there is still a debate on whether NLS1 follow or not the  $M_{BH} - \sigma$  relation found for normal galaxies (e.g., [Tremaine et al. 2002](#)). Some authors found that NLS1 galaxies do not follow this relation, with the majority of the galaxies lying below the  $M_{BH} - \sigma$  relation, with smaller  $M_{BH}$  for a given stellar velocity dispersion (e.g., [Mathur et al. 2001](#); [Grupe & Mathur 2004](#); [Mathur & Grupe 2005a](#); [Zhou et al. 2006](#); [Schmidt et al. 2016](#)). In this scenario, it has been proposed that NLS1 are hosted with galaxies with pseudo-bulges, intrinsically different from normal galaxies ([Mathur et al. 2012](#)). According to our results, NLS1 do follow the  $M_{BH} - \sigma$  relation when the stellar velocity dispersion is directly measured using only the CaT lines or from the integrated spectra (in agreement with [Botte et al. 2005](#) and [Woo et al. 2015](#) among others) and also when we use the core component of  $[\text{OIII}]\lambda 5007$  as a proxy (in agreement with e.g., [Wang & Lu 2001](#); [Komossa & Xu 2007](#); [Cracco et al. 2016](#)).

## 5. Summary and Final Remarks

In this paper we analysed the spectra of a sample of 131 NLS1 galaxies in the Local Universe ( $z < 0.1$ ) taken from the SDSS DR7 through the spectral synthesis technique. It allowed us to infer some properties about the shape and strength of the non-stellar continuum and their relationship with other features of the spectra such as the emission lines. The main results of this paper are summarized as follows:

- For the galaxies in our sample we obtained a median spectral index of  $\beta = -1.6$ , and a median fraction of non-stellar continuum of 0.64. We applied our method to two different samples, one consisting of objects with an expected high AGN contribution to the continuum (QSO), an another one with low AGN contribution to the continuum (Seyfert 2). In the case of QSOs, we obtained a median  $F_{PL} = 0.92$  while for Seyfert 2,  $F_{PL} = 0.19$ .
- NLS1 galaxies are known to have strong FeII emission, we found a range of  $R_{4570}$  between 0.15 and 2 with a median of 0.74. We found no correlation among  $R_{4570}$  and  $F_{PL}$  and only a weak one with  $\beta$ .
- In concordance with previous studies the galaxies in our sample seem to follow the  $M - \sigma$  relation when only the core emission of the  $[\text{OIII}]\lambda 5007$  is considered. The objects are also located on the relation when the stellar velocity dispersion is measured from the CaT lines, and when it is obtained considering the broadening of the whole spectra as is done with STARLIGHT.
- Finally, we found a new correlation between the black hole mass and the fraction of non-stellar contribution to the continuum. Related to this, galaxies with higher black hole masses tend to present a higher amount of non-stellar emission.

In the context of the unified model, this kind of galaxies present intermediate  $F_{PL}$ , lower  $M_{BH}$  and also show lower stellar velocity dispersion, implying that NLS1 are an extension of BLAGNs at the lower mass end.

## Acknowledgements

This work was partially supported by Consejo de Investigaciones Científicas y Técnicas (CONICET) and Secretaría de Ciencia y Técnica de la Universidad Nacional de Córdoba (SecyT). Funding for the SDSS and SDSS-II has been provided by the Alfred P. Sloan Foundation, the Participating Institutions, the National Science Foundation, the U.S. Department of Energy, the National Aeronautics and Space Administration, the Japanese Monbukagakusho, the Max Planck Society, and the Higher Education Funding Council for England. The SDSS Web Site is <http://www.sdss.org/>. The SDSS is managed by the Astrophysical Research Consortium for the Participating Institutions. The Participating Institutions are the American Museum of Natural History, Astrophysical Institute Potsdam, University of Basel, University of Cambridge, Case Western Reserve University, University of Chicago, Drexel University, Fermilab, the Institute for Advanced Study, the Japan Participation Group, Johns Hopkins University, the Joint Institute for Nuclear Astrophysics, the Kavli Institute for Particle Astrophysics and Cosmology, the Korean Scientist Group, the Chinese Academy of Sciences (LAMOST), Los Alamos National Laboratory, the Max-Planck-Institute for Astronomy (MPIA), the Max-Planck-Institute for Astrophysics (MPA), New Mexico State University, Ohio State University, University of Pittsburgh, University of Portsmouth,

Princeton University, the United States Naval Observatory, and the University of Washington. The STARLIGHT project is supported by the Brazilian agencies CNPq, CAPES and FAPESP and by the France-Brazil CAPES/Cofecub program.

## References

- Abazajian, K., Adelman-McCarthy, J. K., Agüeros, M. A., et al. 2005, *AJ*, 129, 1755
- Abazajian, K. N., Adelman-McCarthy, J. K., Agüeros, M. A., et al. 2009, *ApJS*, 182, 543
- An, T., Paragi, Z., Frey, S., et al. 2013, *MNRAS*, 433, 1161
- Barth, A. J., Bennert, V. N., Canalizo, G., et al. 2015, *The Astrophysical Journal Supplement Series*, 217, 26
- Barvainis, R. 1993, *ApJ*, 412, 513
- Benítez, E., Méndez-Abreu, J., Fuentes-Carrera, I., et al. 2013, *ApJ*, 763, 36
- Bian, W. & Zhao, Y. 2004, *MNRAS*, 347, 607
- Bian, W.-H. 2007, in *Astronomical Society of the Pacific Conference Series*, Vol. 373, *The Central Engine of Active Galactic Nuclei*, ed. L. C. Ho & J.-W. Wang, 675
- Botte, V., Ciroi, S., di Mille, F., Rafanelli, P., & Romano, A. 2005, *MNRAS*, 356, 789
- Bruzual, G. & Charlot, S. 2003, *MNRAS*, 344, 1000
- Calderone, G., Nicastro, L., Ghisellini, G., et al. 2017, *MNRAS*, 472, 4051
- Cappellari, M. 2017, *MNRAS*, 466, 798
- Cardelli, J. A., Clayton, G. C., & Mathis, J. S. 1989, *ApJ*, 345, 245
- Cid Fernandes, R., González Delgado, R. M., Storchi-Bergmann, T., Martins, L. P., & Schmitt, H. 2005a, *MNRAS*, 356, 270
- Cid Fernandes, R., Gu, Q., Melnick, J., et al. 2004, *MNRAS*, 355, 273
- Cid Fernandes, R., Mateus, A., Sodré, L., Stasińska, G., & Gomes, J. M. 2005b, *MNRAS*, 358, 363
- Cid Fernandes, Jr., R., Storchi-Bergmann, T., & Schmitt, H. R. 1998, *MNRAS*, 297, 579
- Cracco, V., Ciroi, S., Berton, M., et al. 2016, *MNRAS*, 462, 1256
- Davis, S. W., Woo, J.-H., & Blaes, O. M. 2007, *ApJ*, 668, 682
- Dietrich, M., Crenshaw, D. M., & Kraemer, S. B. 2005, *ApJ*, 623, 700
- Donley, J. L., Rieke, G. H., Alexander, D. M., Egami, E., & Pérez-González, P. G. 2010, *ApJ*, 719, 1393
- Donoso, L., Alonso, M. V., García Lambas, D., et al. 2018, *A&A*, 615, A11
- Ferrarese, L. & Merritt, D. 2000, *ApJ*, 539, L9
- Francis, P. J. 1996, *PASA*, 13, 212
- Francis, P. J., Drake, C. L., Whiting, M. T., Drinkwater, M. J., & Webster, R. L. 2001, *PASA*, 18, 221
- Francis, P. J., Hewett, P. C., Foltz, C. B., et al. 1991, *ApJ*, 373, 465
- Gebhardt, K., Bender, R., Bower, G., et al. 2000, *ApJ*, 539, L13
- Giallongo, E. & Vagnetti, F. 1992, *ApJ*, 396, 411
- Goad, M. R., Korista, K. T., & Ruff, A. J. 2012, *MNRAS*, 426, 3086
- Goodrich, R. W. 1989, *ApJ*, 342, 224
- Greene, J. E. & Ho, L. C. 2005, *ApJ*, 630, 122
- Greene, J. E. & Ho, L. C. 2006, *ApJ*, 641, 117
- Grupe, D., Beuermann, K., Mannheim, K., & Thomas, H. C. 1999, *A&A*, 350, 805
- Grupe, D. & Mathur, S. 2004, *ApJ*, 606, L41
- Heckman, T. M., Kauffmann, G., Brinchmann, J., et al. 2004, *ApJ*, 613, 109
- Kaspi, S., Smith, P. S., Netzer, H., et al. 2000, *ApJ*, 533, 631
- Komossa, S. 2008, in *Revista Mexicana de Astronomía y Astrofísica*, vol. 27, Vol. 32, *Revista Mexicana de Astronomía y Astrofísica Conference Series*, 86–92
- Komossa, S. & Xu, D. 2007, *ApJ*, 667, L33
- Kormendy, J. & Ho, L. C. 2013, *ARA&A*, 51, 511
- Kormendy, J. & Richstone, D. 1995, *ARA&A*, 33, 581
- Kovačević, J., Popović, L. Č., & Dimitrijević, M. S. 2010, *ApJS*, 189, 15
- Lani, C., Netzer, H., & Lutz, D. 2017, *MNRAS*, 471, 59
- León-Tavares, J., Valtaoja, E., Chavushyan, V. H., et al. 2011, *MNRAS*, 411, 1127
- Lynden-Bell, D. 1969, *Nature*, 223, 690
- Lyu, J., Rieke, G. H., & Albers, S. 2016, *ApJ*, 816, 85
- Magorrian, J., Tremaine, S., Richstone, D., et al. 1998, *AJ*, 115, 2285
- Marziani, P., del Olmo, A., D’Onofrio, M., et al. 2018, in *Revisiting narrow-line Seyfert 1 galaxies and their place in the Universe*. 9-13 April 2018. Padova Botanical Garden, 2
- Mateus, A., Sodré, L., Cid Fernandes, R., et al. 2006, *MNRAS*, 370, 721
- Mathur, S. 2000a, *MNRAS*, 314, L17
- Mathur, S. 2000b, *New Astronomy Reviews*, 44, 469
- Mathur, S., Fields, D., Peterson, B. M., & Grupe, D. 2012, *ApJ*, 754, 146
- Mathur, S. & Grupe, D. 2005a, *A&A*, 432, 463
- Mathur, S. & Grupe, D. 2005b, *ApJ*, 633, 688
- Mathur, S., Kuraszekiewicz, J., & Czerny, B. 2001, *New A*, 6, 321
- McLure, R. J. & Dunlop, J. S. 2002, *MNRAS*, 331, 795
- Mullaney, J. R. & Ward, M. J. 2008, *MNRAS*, 385, 53
- Nelson, C. H., Green, R. F., Bower, G., Gebhardt, K., & Weistrop, D. 2004, *ApJ*, 615, 652
- Nelson, C. H. & Whittle, M. 1996, *ApJ*, 465, 96
- Neugebauer, G., Green, R. F., Matthews, K., et al. 1987, *ApJS*, 63, 615
- Nikolajuk, M., Czerny, B., & Gurynowicz, P. 2009, *MNRAS*, 394, 2141
- O’Brien, P. T., Wilson, R., & Gondhalekar, P. M. 1988, *MNRAS*, 233, 801
- Osterbrock, D. E. & Pogge, R. W. 1985, *ApJ*, 297, 166
- Petrosian, V. 1976, *ApJ*, 209, L1
- Pogge, R. W. & Owen, J. M. 1993, *OSU Internal Report* 93-01
- Pol, N. & Wadadekar, Y. 2017, *MNRAS*, 465, 95
- Pu, X., Bian, W., & Huang, K. 2006, *MNRAS*, 372, 246
- Rakshit, S., Stalin, C. S., Chand, H., & Zhang, X.-G. 2017, *ApJS*, 229, 39
- Richstone, D. O. & Schmidt, M. 1980, *ApJ*, 235, 361
- Rodríguez-Ardila, A., Pastoriza, M. G., & Donzelli, C. J. 2000, *ApJS*, 126, 63
- Sargent, W. L. W., Steidel, C. C., & Boksenberg, A. 1989, *ApJS*, 69, 703
- Scharwächter, J., Husemann, B., Busch, G., Komossa, S., & Dopita, M. A. 2017, *ApJ*, 848, 35
- Schlegel, D. J., Finkbeiner, D. P., & Davis, M. 1998, *ApJ*, 500, 525
- Schmidt, E. O. 2019, *PASP*, 131, 037001
- Schmidt, E. O., Ferreira, D., Vega Neme, L., & Oio, G. A. 2016, *A&A*, 596, A95
- Schmidt, E. O., Oio, G. A., Ferreira, D., Vega, L., & Weidmann, W. 2018, *A&A*, 615, A13
- Schmitt, H. R., Storchi-Bergmann, T., & Cid Fernandes, R. 1999, *MNRAS*, 303, 173
- Shapovalova, A. I., Popović, L. Č., Burenkov, A. N., et al. 2012, *ApJS*, 202, 10
- Shields, G. A., Gebhardt, K., Salviander, S., et al. 2003, *ApJ*, 583, 124
- Strauss, M. A., Weinberg, D. H., Lupton, R. H., et al. 2002, *AJ*, 124, 1810
- Sulentic, J. W., Marziani, P., & Dultzin-Hacyan, D. 2000, *Annual Review of Astronomy and Astrophysics*, 38, 521
- Tody, D. 1993, in *Astronomical Society of the Pacific Conference Series*, Vol. 52, *Astronomical Data Analysis Software and Systems II*, ed. R. J. Hanisch, R. J. V. Brissenden, & J. Barnes, 173
- Tremaine, S., Gebhardt, K., Bender, R., et al. 2002, *ApJ*, 574, 740
- Vanden Berk, D. E., Richards, G. T., Bauer, A., et al. 2001, *AJ*, 122, 549
- Vanden Berk, D. E., Shen, J., Yip, C.-W., et al. 2006, *AJ*, 131, 84
- Vazdekis, A., Koleva, M., Ricciardelli, E., Röck, B., & Falcón-Barroso, J. 2016, *MNRAS*, 463, 3409
- Vega, L. R., Asari, N. V., Cid Fernandes, R., et al. 2009, *MNRAS*, 393, 846
- Véron-Cetty, M.-P., Joly, M., & Véron, P. 2004, *A&A*, 417, 515
- Véron-Cetty, M.-P. & Véron, P. 2010, *A&A*, 518, A10
- Véron-Cetty, M.-P., Véron, P., & Gonçalves, A. C. 2001, *A&A*, 372, 730
- Vestergaard, M. 2002, *ApJ*, 571, 733
- Wang, D.-L., Wang, J.-G., & Dong, X.-B. 2009, *Research in Astronomy and Astrophysics*, 9, 1078
- Wang, J.-M. & Zhang, E.-P. 2007, *ApJ*, 660, 1072
- Wang, T. & Lu, Y. 2001, *A&A*, 377, 52
- Wilhite, B. C., Vanden Berk, D. E., Kron, R. G., et al. 2005, *ApJ*, 633, 638
- Wisotzki, L. 2000, *A&A*, 353, 861
- Woo, J.-H., Yoon, Y., Park, S., Park, D., & Kim, S. C. 2015, *ApJ*, 801, 38
- Xu, D., Komossa, S., Zhou, H., et al. 2012, *AJ*, 143, 83
- Xu, D., Komossa, S., Zhou, H., Wang, T., & Wei, J. 2007, *ApJ*, 670, 60
- York, D. G., Adelman, J., Anderson, Jr., J. E., et al. 2000, *AJ*, 120, 1579
- Yuan, W., Zhou, H. Y., Komossa, S., et al. 2008, *ApJ*, 685, 801
- Zhou, H., Wang, T., Yuan, W., et al. 2006, *ApJS*, 166, 128